



ALMA MATER STUDIORUM  
UNIVERSITÀ DI BOLOGNA

ARCHIVIO ISTITUZIONALE  
DELLA RICERCA

## Alma Mater Studiorum Università di Bologna Archivio istituzionale della ricerca

Hierarchical self-assembly and controlled disassembly of a cavitand-based host-guest supramolecular polymer

This is the final peer-reviewed author's accepted manuscript (postprint) of the following publication:

*Published Version:*

Zuccaccia D., Pinalli R., De Zorzi R., Semeraro M., Credi A., Zuccaccia C., et al. (2021). Hierarchical self-assembly and controlled disassembly of a cavitand-based host-guest supramolecular polymer. POLYMER CHEMISTRY, 12, 389-401 [10.1039/d0py01483d].

*Availability:*

This version is available at: <https://hdl.handle.net/11585/828577> since: 2024-01-16

*Published:*

DOI: <http://doi.org/10.1039/d0py01483d>

*Terms of use:*

Some rights reserved. The terms and conditions for the reuse of this version of the manuscript are specified in the publishing policy. For all terms of use and more information see the publisher's website.

This item was downloaded from IRIS Università di Bologna (<https://cris.unibo.it/>).  
When citing, please refer to the published version.

(Article begins on next page)

This is the final peer-reviewed accepted manuscript of:

D. Zuccaccia, R. Pinalli, R. De Zorzi, M. Semeraro, A. Credi,\* C. Zuccaccia, A. Macchioni, S. Geremia,\* E. Dalcanale\*: Hierarchical self-assembly and controlled disassembly of a cavitand-based host-guest supramolecular polymer. *Polymer Chemistry*, vol. 12, pp. 389-401 (2021), DOI: 10.1039/D0PY01483D

The final published version is available online at: <https://dx.doi.org/10.1039/D0PY01483D>

#### Terms of use:

Some rights reserved. The terms and conditions for the reuse of this version of the manuscript are specified in the publishing policy. For all terms of use and more information see the publisher's website.

# Hierarchical Self-assembly and Controlled Disassembly of a Cavitand-based Host-Guest Supramolecular Polymer

Daniele Zuccaccia,<sup>a</sup> Roberta Pinalli,<sup>b</sup> Rita De Zorzi,<sup>c</sup> Monica Semeraro,<sup>d</sup> Alberto Credi,<sup>\*d</sup> Cristiano Zuccaccia,<sup>e</sup> Alceo Macchioni<sup>e</sup>, Silvano Geremia,<sup>\*c</sup> and Enrico Dalcanale<sup>§\*b</sup>

There is a considerable interest in dynamic materials featuring modular components with nano-scale dimensions and controlled responsiveness to external stimuli. Supramolecular polymers are a class of materials that fulfill nicely all these conditions. Here, we present our most recent results regarding a family of host-guest supramolecular polymers that combine the outstanding complexing properties of tetraphosphonate cavitands toward *N*-methylpyridinium guests with molecular switching. The designed monomer is a cavitand featuring four inward facing P=O groups at the upper rim and a single *N*-methylpyridinium unit at the lower rim, forming instantaneously a polymeric species in solution thanks to the high complexation constants measured for these host-guest interactions. This system has been analyzed by NMR spectroscopic and electrochemical techniques. In order to interpret the results of diffusion-sensitive experiments, we took advantage of the X-ray crystal structure obtained for the polymeric species and developed an original treatment of the PGSE data by non-linear fitting. The analysis of the experimental data identified an isodesmic polymerization model at monomer concentration below 20 mM, driven by intrachain host-guest interactions, and an additional level of tetrameric bundle aggregation above 20 mM, due to interchain dipolar and quadrupolar interactions. Two orthogonal disassembly procedures have been implemented: electrochemical reduction for the linear chains and solvent-driven dissolution for the bundles.

## Introduction

Dynamic polymers (DYNAMERS), are drawing the interest of the material scientists community since they display specific responsiveness to external stimuli, adaptation to environmental changes and self-healing capability.<sup>1,2</sup> Supramolecular polymers, held together by non-covalent interactions, are a class of materials that fulfill nicely all these conditions.<sup>3</sup> The basic idea of supramolecular polymers derives directly from the observation of the biological fibrous architectures in the extracellular matrix such as the cell cytoskeleton.<sup>3</sup> Biological systems evolved towards non-covalent polymers due to their flexibility and ability to respond efficiently and in a timely manner to external stimuli, essential requirements to survive in changing environments.<sup>4</sup> Synthetic supramolecular polymers that mimic the properties of the biological systems are exploited in a wide range of technological applications, from biomedical and biomimetic devices<sup>5,6</sup> to photovoltaic and semiconducting materials.<sup>7</sup>

Different approaches have been applied in the design of the building blocks of supramolecular polymers, starting from the first examples of systems based on hydrogen bonding<sup>8</sup> or on metal coordination,<sup>9</sup> followed by self-assembled supramolecular polymers fully or partially created from orthogonal combination of multiple non-covalent binding interactions.<sup>10</sup> A general strategy takes advantage of synergistic interactions with a fast kinetic profile and a behaviour controlled by the thermodynamic constants. In fact, unlikely the covalent polymers that generally display a kinetically controlled

behaviour, in supramolecular polymers, thermodynamics plays a pivotal role in the association of the building blocks and in the behaviour of the stimuli-responsive polymer.

Recently, new studies on supramolecular polymers started to exploit host-guest interactions designing systems with cyclodextrins,<sup>11</sup> cucurbiturils,<sup>12</sup> pillararenes,<sup>13</sup> calixarenes<sup>14,15</sup> and cavitands<sup>16-18</sup> as receptors. Among these, systems based on tetraphosphonate cavitands in their all-inward configuration and ammonium salts proved to be suitable monomers for new supramolecular polymers<sup>19-20</sup> and for polymer blending,<sup>21-22</sup> because of their outstanding complexation properties and high association constants. Previously, we reported the formation in solution and in the solid state of a supramolecular polymer with ditopic building blocks, having a phosphonate cavitand as host functionality and a *N*-methylpyridinium moiety bound to the lower rim of the cavitand as guest functionality.<sup>19</sup> In solution this monomer forms instantaneously a polymer thanks to the high complexation constants ( $K_a \approx 10^7 \text{ M}^{-1}$ ) measured for these host-guest interactions and the responsiveness of these polymers to external stimuli has been verified by addition of a competitive guest (*N*-butylmethylammonium iodide salt,  $K_a \approx 10^{10} \text{ M}^{-1}$ ) for dissociation, followed by base-driven reassembly.<sup>19</sup>

Electrochemical experiments on model systems have shown that one-electron reduction of the *N*-methylpyridinium guests leads to decomplexation.<sup>23</sup> Since the monoelectronic reduction of the investigated guests is reversible, it may be envisaged that the formation and dissociation of such complexes can be electrochemically controlled.

In this work, we demonstrate that the assembly of high molecular weight host-guest polymers proceeds through the

formation of bundles. The aggregation modes of this class of supramolecular polymers is revealed by a variety of spectroscopic and electrochemical measurements, supported by theoretical polymerization models. Bundles formation is triggered by a concentration threshold, above which the aggregation of oligomeric chains is favoured over the isodesmic growth of a single chain. The different nature of the weak interactions involved in the two assembly modes allows to implement orthogonal disassembly procedures in the form of electrochemical reduction for the linear chains and solvent-driven dissolution for the bundles.

## Experimental

**NMR spectroscopy.** One-dimensional  $^1\text{H}$ ,  $^{13}\text{C}$ ,  $^{19}\text{F}$  and  $^{31}\text{P}$  NMR spectra were measured on Bruker DRX 400 spectrometers equipped with a GREAT 1/10 gradient unit and a QNP probe with a Z-gradient coil. Referencing is relative to TMS ( $^1\text{H}$  and  $^{13}\text{C}$ ),  $\text{CCl}_3\text{F}$  ( $^{19}\text{F}$ ), and 85%  $\text{H}_3\text{PO}_4$  ( $^{31}\text{P}$ ). NMR samples were prepared by dissolving a suitable amount of compound in 0.5 mL of the appropriate solvent. All measurements were performed at 296K, unless otherwise stated.

Two-dimensional  $^1\text{H}$ -NOESY and  $^1\text{H}$ -EXSY<sup>24</sup> NMR experiments were acquired by the standard three-pulse sequence or by the PFG version.<sup>25</sup> Two-dimensional  $^{19}\text{F}$ ,  $^1\text{H}$ -HOESY NMR experiments were acquired using the standard four-pulse sequence or the modified version.<sup>26</sup> The number of transients and the number of data points were chosen according to the sample concentration and to the desired final digital resolution. Semi-quantitative  $^1\text{H}$ -NOESY and  $^{19}\text{F}$ ,  $^1\text{H}$ -HOESY NMR spectra were acquired using a 2 s relaxation delay and 800 ms mixing times.

Quantitative  $^1\text{H}$ -EXSY NMR experiments were carried out with a relaxation delay of 5 s and a mixing time ( $\tau_m$ ) ranging from 0.01 s to 0.3 s. For an uncoupled system of spins undergoing chemical exchange between sites A and B, with the simplification of equal spin-lattice relaxation time, the exchange rate constants ( $k_{\text{obs}}$ ) between site A and site B can be estimated by equations (1) and (2)

$$\ln\left(\frac{r+1}{r-1}\right) = k_{\text{obs}} \tau_m \quad (1)$$

$$r = \frac{4X_a X_b (I_{aa} + I_{bb})}{(I_{ab} + I_{ba})} - (X_a - X_b) \quad (2)$$

where  $I_{aa}$ ,  $I_{bb}$ ,  $I_{ab}$  and  $I_{ba}$  represent diagonal- and cross-peak volumes, respectively, and  $X_a$  and  $X_b$  the molar fractions of species A and B.<sup>27</sup> In the present case, A and B denote free tetrakisphosphonate cavitand and tetrakisphosphonate cavitand with encapsulated *N*-methyl-pyridinium. The diagonal- and cross-peak volumes were measured using "XWinNMR" Bruker software after phase and baseline corrections in both dimension. The volume uncertainty was estimated by determining the volume of noise signal in a 'blank region' of the 2D-spectra. Molar fraction  $X_a$  and  $X_b$  were obtained from integration of the corresponding  $^1\text{H}$  NMR spectrum. Linear

regressions of experimental values using equation (1) to estimate  $k_{\text{obs}}$  were performed by means of the software package Microcal Origin 7.0.

**PGSE Measurements.** PGSE NMR measurements were performed by using the standard stimulated echo pulse sequence<sup>28</sup> without spinning.

The dependence of the resonance intensity ( $I$ ) on a constant waiting time and on a varied gradient strength ( $G$ ) is described by Equation (3):

$$I = I_0 \cdot \exp\left[-(\gamma\delta)^2 D_t \left(\Delta - \frac{\delta}{3}\right) G^2\right] \quad (3)$$

where  $I$  is the intensity of the observed spin echo,  $I_0$  is the intensity of the spin echo without gradients,  $D_t$  the translational diffusion coefficient,  $\Delta$  the delay between the midpoints of the gradients,  $\delta$  the length of the gradient pulse, and  $\gamma$  is the magnetogyric ratio. The shape of the gradients was rectangular, their duration ( $\delta$ ) was 5 ms, and their strength ( $G$ ) was varied during the experiments. Different values of  $\Delta$  (120, 300, 600, 1800 ms), "nt" (number of transients) and number of different gradient strengths ( $G$ ) were used for different samples. In the case of a single species or a monodisperse distribution of species in fast exchange in the diffusion NMR timescale ( $\Delta$ ),  $D_t$  can be obtained from linear regression of the semi-logarithmic plots of  $\ln(I/I_0)$  vs  $G^2$  by measuring the instrumental constant, using a sample of HDO (5%) in  $\text{D}_2\text{O}$  (known diffusion coefficient in the range 274- 318K)<sup>29-30</sup> in the same exact condition as the sample of interest. Temperature and gradient pulse fluctuations as well as variation of the fluid viscosity ( $\eta$ ) with increasing sample concentration were taken into account using tetrakis-(trimethylsilyl) silane (TMSS) as internal standard.  $D_t$  data were treated as described in the literature.<sup>28</sup> The measurement uncertainty was estimated to be approximately 3-4% in  $D_t$ .

**Fitting.** Evaluation of the translational diffusion coefficients, calculation of the distribution of polymeric species and fitting of the experimental PGSE data to optimize the polymerization parameters have been performed using the software Octave<sup>31</sup> and, in particular, the package Optim. Scripts developed for this analysis are deposited in Supplementary Information.

**Electrochemical experiments.** Cyclic voltammetry (CV) and differential pulse voltammetry (DPV) experiments were carried out in argon-purged  $\text{CH}_2\text{Cl}_2$  (Romil Hi-Dry) at room temperature with an Autolab 30 multi-purpose instrument interfaced to a PC. The working electrode was a glassy carbon electrode (Amel; 0.07  $\text{cm}^2$ ), the counter electrode was a Pt wire, separated from the solution by a frit, and an Ag wire was employed as a quasi-reference electrode. Ferrocene was present as an internal standard ( $E_{1/2} = +0.46$  V vs. SCE). Tetrabutylammonium hexafluorophosphate was employed as the supporting electrolyte, and the examined potential window was comprised between  $-2.0$  V and  $+2.0$  V vs SCE. The IR compensation implemented within the Autolab 30 was used, and every effort was made throughout the experiments to minimise the resistance of the solution. In any instance, the full electrochemical reversibility of the voltammetric wave of ferrocene was taken as an indicator of the absence of

uncompensated resistance effects. For reversible processes the half-wave potential values were calculated from an average of CV and DPV experiments, whereas the redox potential values in the case of irreversible processes were estimated from the DPV peaks. Experimental errors: potential values, 10 mV for reversible processes, 20 mV for irreversible processes. Spectroelectrochemical measurements were performed in situ with a custom-made optically transparent thin-layer electrochemical (OTTLE) cell by using an Autolab 30 potentiostat and an Agilent Technologies 8543 diode array spectrophotometer. The working and counter electrodes were Pt minigrids, and the quasi-reference electrode was an Ag wire; all the electrodes were melt-sealed into a polyethylene spacer. The thickness of the layer, determined by spectrophotometry, was about 180  $\mu\text{m}$ .

## Results and discussion

The family of host-guest supramolecular polymers formed by ditopic building blocks, having a phosphonate cavitand as host functionality and a *N*-methylpyridinium moiety bound to the lower rim of the cavitand as guest functionality has been designed, prepared and characterized previously.<sup>19</sup> The crystal structure of the homopolymer **11** (Scheme 1, Figure 1) gives evidence of the two major interactions responsible for the complexation: a multiple ion-dipole interaction between the inward-facing P=O groups and the positively charged methylpyridinium moiety, and directional hydrogen bonds involving the acidic methyl group with the  $\pi$ -basic cavity (cation- $\pi$  interaction) and the *ortho* H-pyridinium atoms with two opposite P=O groups. The crystal packing (Figure 1) shows that each linear polymeric chain packs against other four antiparallel chains. Furthermore, in the crystallographic structure, the counterions are located in between the lower rim and the alkyl chains, close to the methylpyridinium fragment. The characterization in solution performed by ITC (Isothermal Titration Calorimetry) on **2•3PF<sub>6</sub>** (a suitable model of a single monomer-monomer connection) indicates a high association constant ranging from  $10^4$  in MeOH to  $10^7$  M<sup>-1</sup> in dichloromethane. Finally, by static light scattering in batch off-line model the weight-averaged molecular weight of polymer was determined only at medium-low concentration values (below 20 mM) indicating a degree of polymerization of about 18 units.<sup>19</sup>

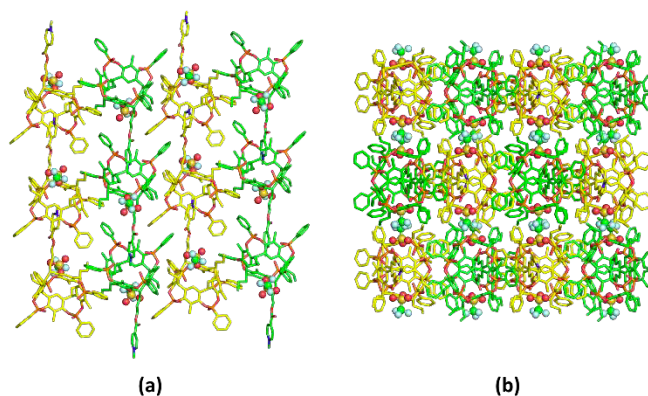
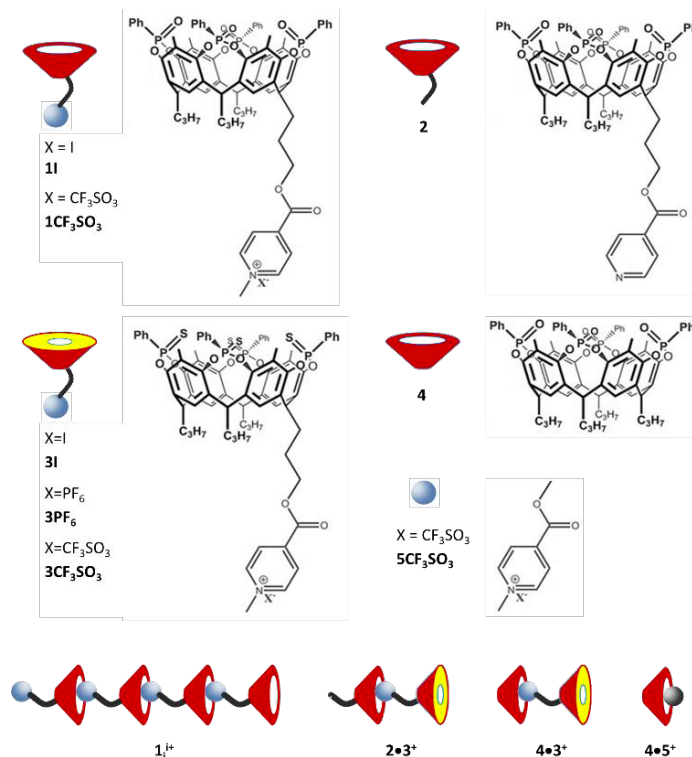


Figure 1. Crystal packing of **1CF<sub>3</sub>SO<sub>3</sub>** homopolymer as viewed (a) perpendicular to the linear polymeric chains and (b) along the polymeric chains. Chains with the dipolar moment pointing in opposite direction are shown in different colors. (Triflate ions are represented in ball and sticks).

The aim of this study is to deepen our understanding about the solution behaviour of this class of ionic supramolecular homopolymers by exploiting an integrated experimental approach based on PGSE (pulsed field gradient spin-echo),<sup>32</sup> NOE<sup>33</sup> and EXSY (exchange spectroscopy)<sup>27</sup> NMR experiments as well as cyclic voltammetry (CV), differential pulse voltammetry (DPV) and spectroelectrochemical measurements.



Scheme 1. The ionic host-guest cavitands investigated by electrochemical and NMR experiments.

In detail, the supramolecular solution structures of ionic host-guest cavitands **11**, **1CF<sub>3</sub>SO<sub>3</sub>** and **31** and dimer **2•3PF<sub>6</sub>** (Scheme 1) were investigated.

## Supramolecular solution structure by NOE Measurements

The structure of supramolecular polymers in solution was investigated by using a combination of homo- and heteronuclear Overhauser NMR experiments. In the  $^1\text{H}$ -NOESY NMR spectrum of  $1\text{CF}_3\text{SO}_3$  in  $\text{CDCl}_3$  (Figure 2), a strong contact was observed between **Ar-Me** and **o-PyMe** and a weak/medium one between **Py-Me** and **Ar-H** resonances. Both NOE interactions, not expected if the monomeric  $1\text{CF}_3\text{SO}_3$  would be the main species in solution, indicate close proximity between the pyridinium and phosphonate fragments, confirming formation of supramolecular adducts in solution. In particular, **MePy<sup>+</sup>** moieties are located near the **P=O** groups: from this position the pyridine protons of one unit, being far away from their cavitand skeleton, can interact with the Ar protons of the cavitand skeleton belonging to another unit.

The anion-cation relative position in solution for the homopolymer  $1\text{CF}_3\text{SO}_3$  was determined by detecting dipolar interionic interactions in the  $^{19}\text{F}$ , $^1\text{H}$ -HOESY NMR spectrum at room temperature (Figure 3). Normalization of the experimental cross peaks intensities, by taking into account the number of equivalent nuclei,<sup>26</sup> gives the results reported in Table 1. Strong contacts were observed between F-atoms of the counterion and aliphatic chain resonances and **Ar-H** resonances of the cavitand fragment. Very weak contacts were detected with **Ar-Me** and **Py-Me** resonances, whereas the anion did not show any interaction with protons of the phenyl ring bonded to the phosphorous. This pattern of heteronuclear Overhauser contacts, together with the trend of intensities reported in Table 1, indicates that the  $\text{CF}_3\text{SO}_3^-$  is mainly located on the plane of the cavitand within the aliphatic chains, as shown in Figure 3. From this position the anion has the possibility to weakly interact with Me-Py and the Ar-Me protons. This cation-anion relative position is the same observed in the solid state structure of the homopolymer.<sup>19</sup>

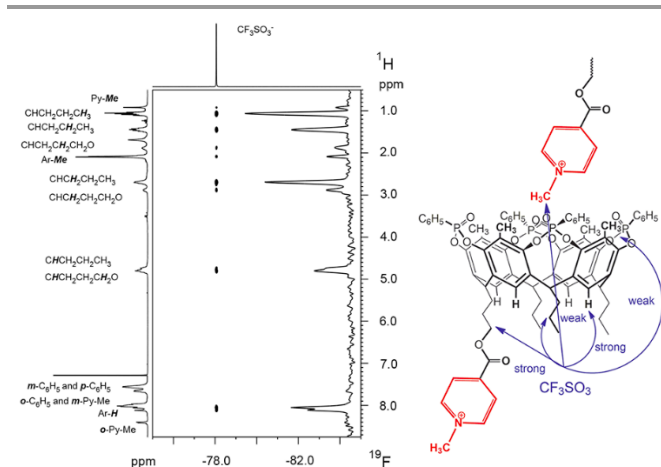


Figure 2. A section of the  $^1\text{H}$ -NOESY NMR spectrum (400.13 MHz, 296 K,  $\text{CDCl}_3$ ) of  $1\text{CF}_3\text{SO}_3$ .

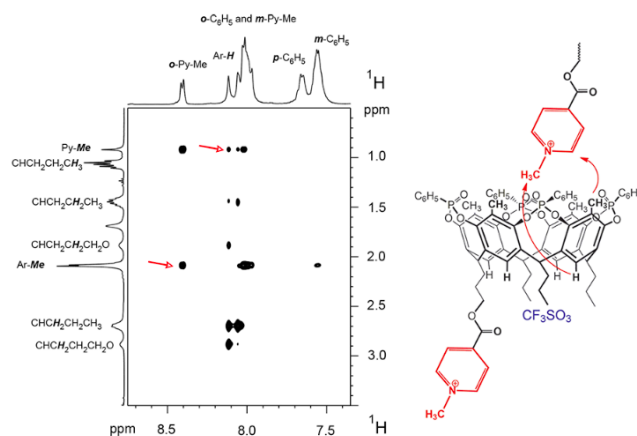


Figure 3.  $^{19}\text{F}$ , $^1\text{H}$ -HOESY NMR spectrum (376.65 MHz, 296K,  $\text{CDCl}_3$ ) of complex  $1\text{CF}_3\text{SO}_3$ . On the right the column projection is reported.

The kinetic stability of polymers **1I**, i. e. the rate of formation and breaking of the supramolecular polymer, is an additional key aspect to take into account when describing their solution behaviour. Since solutions of **1I** display only one set of NMR resonances, such information cannot be easily derived. It can be, nevertheless, obtainable using a model solution system consisting of  $3\text{PF}_6$  and two equivalents of **2** (Scheme 1), exploiting the much lower tendency of  $3\text{PF}_6$  to form homopolymers.<sup>19</sup> Under these conditions, two well-separated  $^1\text{H}$  NMR resonances are observed for the **Ar-Me** moiety of **2**, one related to  $2\cdot 3\text{PF}_6$  and the other to free **2**. Monitoring the chemical exchange between these two resonances by  $^1\text{H}$ -EXSY NMR experiments allowed to extract the rate constant ( $k_{\text{obs}}$ ) for the interconversion between free **2** and  $2\cdot 3\text{PF}_6$ .  $k_{\text{obs}}$  was found to be equal to  $1.7\text{ s}^{-1}$ ,  $45\text{ s}^{-1}$  and  $6.3\text{ s}^{-1}$  in  $\text{CDCl}_3$  at 0.3 mM, in  $\text{CDCl}_3$  at 2.1 mM and in  $\text{CDCl}_3/\text{CD}_3\text{OD}$  (92/8) at 0.3 mM, respectively. This indicates that formation-rupture of supramolecular polymers are accelerated by increasing concentrations of monomer whereas a slight increase of  $k_{\text{obs}}$  is observed when a small amounts of  $\text{CD}_3\text{OD}$  is added.

Table 1. Relative heteronuclear Overhauser intensities determined by arbitrarily fixing at 1 the intensity of the NOE heteronuclear Overhauser contact between the anion resonances and **Ar-H** resonance.

	$1\text{CF}_3\text{SO}_3$
Ar-H	1
$\text{CHCH}_2\text{CH}_2\text{CH}_3$ and $\text{CHCH}_2\text{CH}_2\text{CH}_2\text{O}$	0.62
$\text{CHCH}_2\text{CH}_2\text{CH}_2\text{O}$	0.49
$\text{CHCH}_2\text{CH}_2\text{CH}_3$	0.95
Ar-Me	0.12
$\text{CHCH}_2\text{CH}_2\text{CH}_2\text{O}$	0.28
$\text{CHCH}_2\text{CH}_2\text{CH}_3$	0.65
$\text{CHCH}_2\text{CH}_2\text{CH}_3$	0.99
Py-Me	0.08

## Supramolecular solution structure by PGSE NMR experiments

Additional information on the solution behaviour of the homopolymer **1I** can be obtained by PGSE diffusion NMR measurements which allow to get information on the average size of the supramolecular aggregates and, consequently, on the chemical origin of self-aggregation.<sup>34</sup> Initially, diffusion experiments were targeted for the homopolymer **1I** as a function of concentration in CDCl<sub>3</sub> (1.5 mM, 5.5 mM, 10.5 mM, 22.3 mM, 41.0 mM, 64.7 mM, 88.0 mM, 147.0 mM). For such a series of measurements, we unexpectedly found that the standard plots of  $\ln(I/I_0)$  versus  $G^2$  showed sizable curvature at all investigated concentration: average values of the diffusion coefficient ( $D_t$ ) cannot be obtained by linear regression of experimental data and a different approach is necessary in order to obtain information on the self-aggregation tendency (see below). Linear trends are expected in the case of a single species or a monodisperse distribution of species in fast exchange in the PGSE NMR timescale ( $\Delta$ ). Nevertheless, and <sup>1</sup>H-EXSY measurements indicate that exchange occurs on the same time-scale of diffusion, suggesting that **1I** is present in the form of a polydispersed distribution in slow exchange in the NMR timescale. This is reasonably due to the action of more than one type of self-assembly motif. The simplest hypothesis is to consider that formation of linear host-guest chains is coupled with further self-organization of the chains into bundles which are held together by inter-chain electrostatic interactions as observed in the solid state structure of **1CF<sub>3</sub>SO<sub>3</sub>** (Figure 1). The PGSE methodological approach was tested by performing some measurements on diluted CDCl<sub>3</sub> solutions of the dimer **2•3PF<sub>6</sub>**, the stopper **3I**, and on solutions of **1I** in CDCl<sub>3</sub>/CD<sub>3</sub>OD (92/8) solvent mixture. The results are reported in Table 2. In all cases, linear trends are observed and fitting according to equation 3 allowed to obtain  $D_t$  values that were interpolated with equation 13 (see next sections), showing the dependence of  $D_t$  vs  $i$ . The apparent number of monomers ( $i$ ) in the supramolecular polymer as a function of concentration was obtained (Table 2). The values of  $i$  obtained (entries 5–6 in Table 2, for **2•3PF<sub>6</sub>**, and entry 1 in Table 2, for **3I** at low concentration) are in good agreement with the predictions of Equation 12 (see next sections). PGSE measurements for **3I** at higher concentrations (entries 2–4 in Table 2) clearly indicate the formation of supramolecular aggregates of few units, since values of  $D_t$  obtained for this concentrations are lower than  $4.66 \cdot 10^{-10} \text{ m}^2\text{s}^{-1}$  (the theoretical value for the monomer), consistently with its low tendency to aggregate. Similarly to **3I** and differently from the behaviour in pure CDCl<sub>3</sub>, plots of  $\ln(I/I_0)$  versus  $G^2$  are also linear for solutions of **1I** in CDCl<sub>3</sub>/CD<sub>3</sub>OD (92/8, entries 7–10, Table 2). It is reasonable to hypothesize that the presence of a minimal amount of CD<sub>3</sub>OD in CDCl<sub>3</sub> tends to disfavour the additional self-organization of the chains into bundles, as will be further discussed below (cyclic voltammetry, differential pulse voltammetry and spectroelectrochemical measurements).

Table 2. Diffusion coefficients ( $D_t \cdot 10^{-10} \text{ m}^2\text{s}^{-1}$ ), number of monomer units  $i$ , for compounds **1I**, **3I** and dimer **2•3PF<sub>6</sub>** as a function of concentration and solvent ( $C$ , mM).

Entry ( $\Delta$ , ms)	Solvent	C (mM)	$D_t$	$i$
<b>3I</b>				
1 (120)	CDCl <sub>3</sub>	0.2	3.80	1.8
2 (120)	CDCl <sub>3</sub>	1.0	3.15	2.6
3 (120)	CDCl <sub>3</sub>	11.0	2.41	4.2
4 (120)	CDCl <sub>3</sub>	20.0	2.22	4.9
<b>2•3PF<sub>6</sub></b>				
5 (120)	CDCl <sub>3</sub>	1.0	3.52	2.0
6 (120)	CDCl <sub>3</sub>	3.0	3.40	2.2
<b>1I</b>				
7 (120)	CDCl <sub>3</sub> /CD <sub>3</sub> OD (92/8)	5.5	1.72	7.3
8 (120)	CDCl <sub>3</sub> /CD <sub>3</sub> OD (92/8)	13.4	1.33	10.8
9 (120)	CDCl <sub>3</sub> /CD <sub>3</sub> OD (92/8)	22.3	1.01	16.0
10 (120)	CDCl <sub>3</sub> /CD <sub>3</sub> OD (92/8)	41.4	0.72	25.5

As stated above, the non-linear trends of  $\ln(I/I_0)$  versus  $G^2$  plots, observed for **1I** in CDCl<sub>3</sub> at different concentrations, suggest the presence of a polydispersed distribution in slow exchange and requires a different treatment of the experimental data. In the case of polydispersed distribution, the intensity of PGSE signal depends on the diffusion coefficient of each species and on the concentration of the monomer responsible for the resonance signal and present in oligomers in solution, therefore:

$$I = \sum_i I_{0,i} \cdot \exp\left[-(\gamma\delta)^2 D_i \left(\Delta - \frac{\delta}{3}\right) G^2\right] \quad (4)$$

Considering that the initial intensity of the signal, i.e. at field gradient value equal to zero, is proportional to the molar fraction of each polymeric species, multiplied by the number of monomers present in the polymer, Equation (4) can be written as:

$$I = I_0 \sum_i \frac{C_i \cdot i}{C_{tot}} \cdot \exp\left[-(\gamma\delta)^2 \left(\Delta - \frac{\delta}{3}\right) D_i G^2\right] \quad (5)$$

In order to provide a fitting of experimental data using Equation (5), the values of the concentration of each polymeric species ( $C_i$ ) and the hydrodynamic translational diffusion coefficients ( $D_i$ ) are required.

### Distribution of polymeric species

Different models for the polymerization were evaluated, each of them corresponding to a different distribution of the polymeric species.

The first model, called Sequential Equal K (SEK) model,<sup>35</sup> consists in a stepwise polymerization for which every subsequent step has the same constant,  $K_{SEK}$ , as the previous ones (isodesmic model).

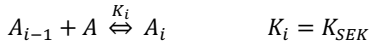
The second model for the polymerization equilibrium that was taken into account is the Attenuated K (AK) model.<sup>35</sup> In this model, the thermodynamic constants for the formation of increasingly longer species decrease proportionally to  $1/i$ . The results obtained with these two simple linear polymerization models, the X-ray structures and the electrochemistry experiments suggested the possibility of a

further aggregation process with formation of supramolecular bundles held together by dipolar and quadrupolar interactions between antiparallel polymeric chains (see below). The SEK model was implemented with tetrameric aggregation equilibria having thermodynamic constants proportional to the number of monomers  $i$  of the linear polymer involved in the formation of antiparallel four-strain bundles (third model: SEK-TAi) or proportional to the fourth power of  $i$  (fourth model: SEK-TAi<sup>4</sup>). These hypotheses are in line with the expected increase of dipolar energy contribution with the increase of the length of the polymer involved in the formation of supramolecular bundles.

In the linear polymerization process of the SEK model the following chemical equations apply:



... ..



where  $A$  is the monomer, while  $A_i$  is the oligomeric specie formed by  $i$  monomers.

From these equilibrium equations, concentrations for the single polymeric species can be obtained depending on free monomer concentration in solution,  $C_1$  and SEK constant:

$$C_i = \frac{(C_1 K_{SEK})^i}{K_{SEK}} \quad (6)$$

For simplicity, we considered only the tetrameric aggregation of oligomeric species with the same number of monomers. Oligomeric species formed by  $i$  monomers are involved in the following equilibrium:



where the tetrameric aggregation constant is assumed proportional to the length of the polymeric chain in the SEK-TAi model.

From these equilibrium equations, concentration for the tetrameric species,  $C_{i4}$  can be obtained depending on the concentration of the polymeric chain with  $i$  monomers,  $C_i$  and the tetrameric aggregation constant,  $K_{TA}$

$$C_{i4} = C_i^4 K_{TAi} = C_i^4 i K_{TA}$$

From equation 6 the concentration for the tetrameric species,  $C_{i4}$  can be expressed in term of concentration of the free monomer in solution,  $C_1$ :

$$C_{i4} = \frac{(C_1 K_{SEK})^{4i} i K_{TA}}{K_{SEK}^4} \quad (7)$$

The total concentration of the monomer  $C_t$  can be obtained as a sum of single oligomer concentrations multiplied by their length,  $i$ , plus the concentration of tetrameric species multiplied

by the number of monomers in the aggregate, i.e. four times the length of a single chain:

$$\begin{aligned} C_t &= \sum_{i=1}^{\infty} i C_i + 4i C_{i4} \\ &= \sum_{i=1}^{\infty} i \frac{(C_1 K_{SEK})^i}{K_{SEK}} + 4i \frac{(C_1 K_{SEK})^{4i} i K_{TA}}{K_{SEK}^4} \\ &= \frac{1}{K_{SEK}} \sum_{i=1}^{\infty} i (C_1 K_{SEK})^i + \frac{4K_{TA}}{K_{SEK}^4} \sum_{i=1}^{\infty} i^2 (C_1 K_{SEK})^{4i} \end{aligned}$$

both series converge under the condition  $K_{SEK} C_1 < 1$  to:

$$C_t = \frac{C_1}{(1 - K_{SEK} C_1)^2} + \frac{4K_{TA} (K_{SEK} C_1)^4 [(K_{SEK} C_1)^4 + 1]}{K_{SEK}^4 [1 - (K_{SEK} C_1)^4]^3} \quad (8)$$

From Equation (8), the concentration of the free monomer in solution,  $C_1$  can be evaluated knowing  $C_t$ ,  $K_{SEK}$  and  $K_{TA}$  values. The distribution of all polymeric species in the SEK-TAi model is calculated using Equations (6) and (7).

For the fourth model, SEK-TAi<sup>4</sup>, the tetrameric aggregation constant is assumed proportional to the fourth power of the number of monomers:



The distribution of the tetrameric species,  $C_{i4}$  is

$$C_{i4} = C_i^4 i^4 K_{TA4}$$

and considering Equation (6):

$$C_{i4} = \frac{(C_1 K_{SEK})^{4i} i^4 K_{TA4}}{K_{SEK}^4} \quad (9)$$

For the SEK-TAi<sup>4</sup> model, the total concentration of the monomer  $C_t$  can be obtained as:

$$\begin{aligned} C_t &= \sum_{i=1}^{\infty} i C_i + 4i C_{i4} \\ &= \sum_{i=1}^{\infty} i \frac{(C_1 K_{SEK})^i}{K_{SEK}} + 4i \frac{(C_1 K_{SEK})^{4i} i^4 K_{TA4}}{K_{SEK}^4} \\ &= \frac{1}{K_{SEK}} \sum_{i=1}^{\infty} i (C_1 K_{SEK})^i + \frac{4K_{TA4}}{K_{SEK}^4} \sum_{i=1}^{\infty} i^5 (C_1 K_{SEK})^{4i} \end{aligned}$$

the series converge under the condition  $K_{SEK} C_1 < 1$  to:

$$C_t = \frac{C_1}{(1 - a)^2} + \frac{4K_{TA4} (a^{20} + 26a^{16} + 66a^{12} + 26a^8 + a^4)}{K_{SEK}^4 (1 - a^4)^6}$$

$$a = K_{SEK} C_1 \quad (10)$$

The concentration of the free monomer in solution,  $C_1$  can be obtained from Equation (10) knowing  $C_t$ ,  $K_{SEK}$  and  $K_{TA4}$  values. The distribution of all polymeric species in the SEK-TAi<sup>4</sup> model is calculated from Equations (6) and (9).

Distributions of polymeric species according to the SEK, AK, SEK-TAi and SEK-TAi<sup>4</sup> models were obtained using the software Octave<sup>31</sup> and *ad hoc* designed algorithms (see Supplementary Information).

### Evaluation of the hydrodynamic translational diffusion coefficients based on the crystallographic structure

In order to obtain the hydrodynamic translational diffusion coefficients of the species in solution used in equation (5), some hypothesis on  $D_i$  should be made. The X-ray crystallographic structure reported previously.<sup>19</sup> (Figure 1) shows the geometry of polymer formation and allows calculation of volumes and dimensions of oligomers. Using coordinates from the crystallographic 3D model and the software HYDRO,<sup>36</sup> we calculated  $D_i$  for the **1CF<sub>3</sub>SO<sub>3</sub>** monomer and for its oligomers. The structure of all the oligomers was assumed to be linear, similarly to that seen in the crystal.<sup>19</sup> Confirmation of the retention of this structure in solution comes from NOE and HOE techniques (vide infra). The tetraphosphonate cavitand can interpose between the methyl-pyridinium and the anion leading to the formation of the supramolecular linear polymer. With HYDRO, the first 11 hydrodynamic translational diffusion coefficients,  $D_i$ , were calculated, for oligomers formed by up to 11 monomers. For a larger assembly, Perrin's law was applied to calculate the behaviour of  $D_i$  with  $i > 11$ .<sup>37</sup>

Considering the crystallographic structure, a prolate model can be used to approximate the polymer cylindrical shape and the axial ratio for the polymer with polymerization degree of  $i$ ,  $p_i$ , is:

$$p_i = \frac{a_{\text{mono}} \cdot i}{b} \quad (10)$$

where  $a_{\text{mono}}$  is the dimension of the monomer in the elongation direction and  $b$  the dimension in the perpendicular direction. For each polymeric species, the Perrin  $S_i$  factor can be evaluated as:

$$S_i = 2 \frac{\text{arctanh } \xi_i}{\xi_i} \quad \text{with} \quad \xi_i = \frac{\sqrt{|p_i^2 - 1|}}{p_i} \quad (11)$$

Considering the monomer as an approximately spherical object,  $a_{\text{mono}}$  equals to  $b$ ,  $p_1$  equals to 1 and  $S_1$  has the limit value of 2. According to Perrin, Einstein and Stokes' equations, the hydrodynamic translational diffusion coefficient is expressed as:

$$D_i = \frac{k_B T}{6\pi\eta \sqrt[3]{\frac{3V_i}{4\pi}} \left( \frac{2 \sqrt[3]{p_i^2}}{S_i} \right)} \quad (12)$$

The volume of the whole polymer can be considered as the volume of a cylinder with the height increasing with  $i$ . From Equation 12, the dependency of  $D_i$  from  $i$  can be written as

$$D_i = \frac{D_1 \cdot S_i}{2 \sqrt[3]{i \cdot p_i^2}} \quad (13)$$

The value of  $D_1$  was optimized from the values of  $D_i$  calculated using HYDRO, with  $i$  from 2 to 11, applying the function *nlinfit* of the software Octave,<sup>31</sup> i.e. a nonlinear regression (see S.I.). Values calculated from Perrin's equations for the translational diffusion coefficients,  $D_i$ , were in good agreement with those obtained using the software HYDRO (Figure S1). With the same algorithm based on Perrin's equations, values of  $D_i$  were calculated for polymeric species up to  $i=10,000$ .

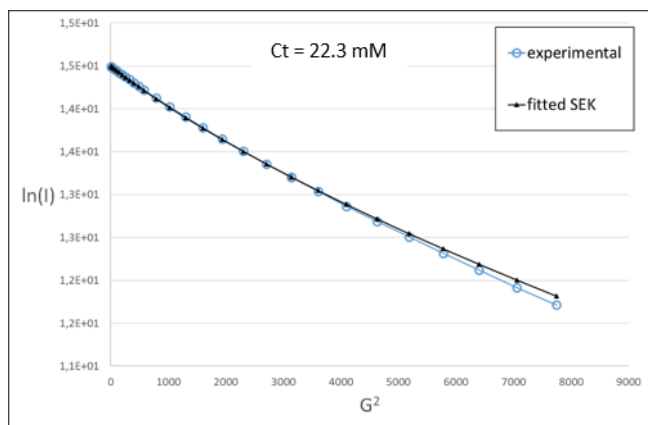
### Non-linear fitting of the PGSE data at different concentrations

Non-linear fittings of the PGSE data were performed using Equation (5), distributions calculated for different models and hydrodynamic translational diffusion coefficients, in order to obtain the thermodynamic constants for each model. In particular, the function *nlinfit* of Octave was used to fit the experimental data of the resonance intensity  $I$ , against the square of the field gradient  $G^2$ , varying the thermodynamic constants and the resonance intensity at  $G=0$   $I_0$ , for 8 different total concentrations of the monomer,  $C_t$  (mM). Figure 4 shows the fitting of two series of data, at concentrations 22.3 mM and 147 mM, respectively, considering a polymerization that follows the SEK model.

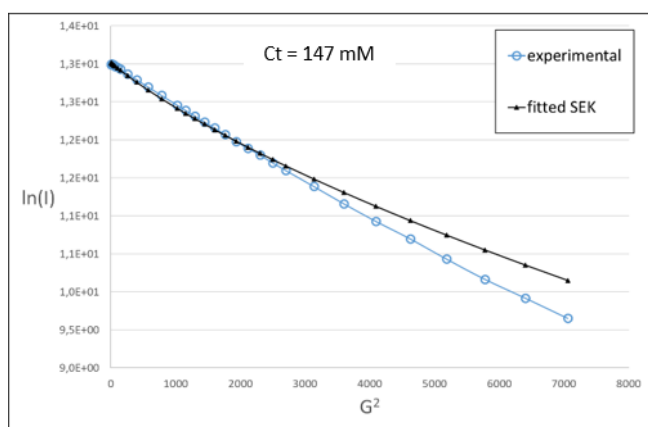
The fitting shows a good agreement for low monomer concentrations (Figure 4a), but it gradually worsens increasing the monomer concentrations (Figure 4b). Figures S2 and S3 show the fitting of PGSE data at different concentrations according to the SEK model and Figure S4 shows the polymeric distributions for each concentration, obtained using the  $K_{\text{SEK}}$  value optimized for each series of data (Table S1).

This fitting procedure was also performed using the AK model. However, in this case the fitting is severely worse than that obtained with the SEK model (see SI, Figures S5, S6 and S7) for the higher monomer concentrations used in the experiments.

The values of  $K_{\text{SEK}}$  optimized against the PGSE data series are slightly different at different concentrations of monomer, as shown in Figure 5. Values of  $K_{\text{SEK}}$  range from a minimum of  $6.1 \times 10^3 \text{ M}^{-1}$  at low concentration of monomer to a maximum of  $7.1 \times 10^4 \text{ M}^{-1}$ . This last value is in agreement with the  $K_a$  determined via ITC for **4** with methyl pyridinium(MePy<sup>+</sup>) iodide in methanol ( $7.1 \times 10^4 \text{ M}^{-1}$ ).<sup>38</sup> In particular,  $K_{\text{SEK}}$  values are fairly constant up to a monomer concentration of 20 mM and then begin to grow linearly. The values of the calculated average degree of polymerization obtained from distributions of polymeric species at low concentration of **11** (Figure 6) are in good agreement with the number of monomer units  $i$  obtained by linear fit of PGSE data collected in the presence of methanol (Table 2). These data suggest that at low concentration of monomer (and in presence of methanol) the formation of linear supramolecular chains, as observed in the solid state, is the dominant self-aggregation process. This behaviour is also confirmed by the SLS measurements.<sup>19</sup> Instead, when the concentration of monomer is higher than 20 mM, other aggregation modes intervene, increasing the apparent value of  $K_{\text{SEK}}$  up to 10 times (Figure 5). This additional aggregation mode is highlighted by the comparison between the values of the calculated average degree of polymerization obtained in the optimization of each series with respect to the trend-line calculated with the minimum  $K_{\text{SEK}}$  constant ( $6.10 \times 10^3 \text{ M}^{-1}$ ) obtained at low concentration of **11**, where aggregation processes should be negligible (Figure 6). For the highest monomer concentration, namely 147 mM, the average degree of polymerization is 3.4 times higher than the trend-line ( $i = 103$  and 30.5, respectively, Figure 7).



(a)



(b)

Figure 4. Experimental (blue circles) and fitted (black triangles) data trend of  $\ln(i)$  versus  $G^2$  for 1I. (a) at 22.3 mM in  $\text{CDCl}_3$  ( $K_{\text{SEK}} = 1.18 \cdot 10^4 \text{ M}^{-1}$ ); (b) at 147 mM in  $\text{CDCl}_3$ . ( $K_{\text{SEK}} = 7.15 \cdot 10^4 \text{ M}^{-1}$ )

A possible explanation for this behaviour is the formation of supramolecular bundles held together by dipolar and quadrupolar interactions between antiparallel polymeric chains, as observed in the solid state (Figure 1).

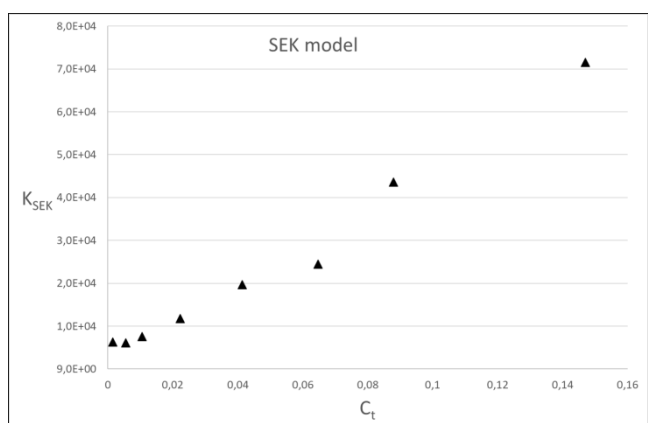


Figure 5. Optimized values of  $K_{\text{SEK}}$  obtained for different monomer molar concentration of 1I in  $\text{CDCl}_3$ .

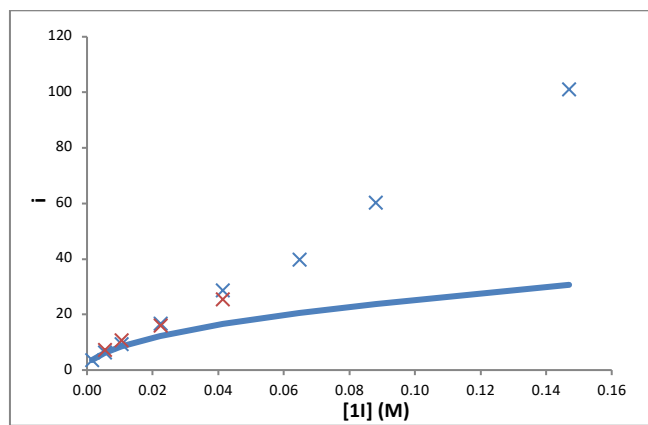


Figure 6. Comparison between the calculated average degree of polymerization obtained from distributions of polymeric species with optimized SEK constants (blue cross) and the number of monomer units  $i$  obtained by linear fit of PGSE data collected in the presence of methanol (red cross). The full line represents the trend-line of the SEK model calculated with the minimum constant of  $6.1 \cdot 10^3 \text{ M}^{-1}$ .

The minimal aggregations in agreement with the apparent degree of polymerization (3.4 times higher than the trend-line, Figure 6) are bundles composed by four antiparallel linear polymeric chains. The antiparallel organization is suggested by the crystal packing, and the formation of supramolecular bundles is supported by electrochemical measurements (vide infra).

Two new models (SEK-TAi and SEK-TAi<sup>4</sup>) were developed in order to take into account the formation of such "secondary" bundle-like structures in equilibrium with the non-aggregated polymer chains. Despite the oversimplification of the aggregation process present in these two new models, a significant improvement in the fitting of experimental PGSE data was observed in both cases (see SI, Figures S8, S9 and S10 for SEK-TAi model and Figures S11, S12 and S13 for SEK-TAi<sup>4</sup> model). The SEK-TAi<sup>4</sup> model with the thermodynamic constant of tetrameric aggregation proportional to the fourth power of  $i$  reproduces better the experimental data than the SEK-TAi model with the  $K_{\text{TA}i}$  proportional to  $i$ , particularly at high concentration of the monomer (Figure 7). The distribution of all polymeric species in the SEK-TAi<sup>4</sup> model can be calculated from the  $K_{\text{SEK}}$  and  $K_{\text{TA}4}$  values. The speciation curves (Figure 8) calculated with the  $K_{\text{SEK}}$  and  $K_{\text{TA}4}$  values obtained in the fitting procedure of the experimental PGSE measurements with a total monomer concentration  $C_t$  of 147 mM, evidence the predominance of the aggregation process of the linear polymeric chains in bundles. The maximum concentration is calculated for a bundle of four linear chains each one formed by 31 monomeric units (Figure 8). The comparison between the calculated average degree of polymerization obtained from distributions of polymeric species in four different models, i.e. SEK, AK, SEK-TAi and SEK-TAi<sup>4</sup> at different concentrations of monomer is shown in Figure 9. The SEK models implemented with a tetrameric aggregation process (SEK-TAi and SEK-TAi<sup>4</sup>), which fit better the experimental PGSE data at higher monomer concentrations, show calculated average degree of polymerization significantly higher with respect to the pure SEK model.

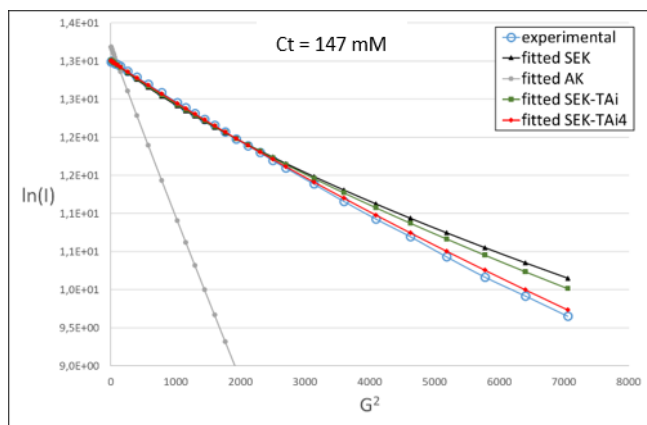


Figure 7. Comparison between the fitting of PGSE experimental data (blue circles) obtained with four different models, i.e. SEK (black triangles), AK (grey circles), SEK-TAi (green squares) and SEK-TAi<sup>4</sup> (red diamonds), for a monomer concentration of 147 mM.

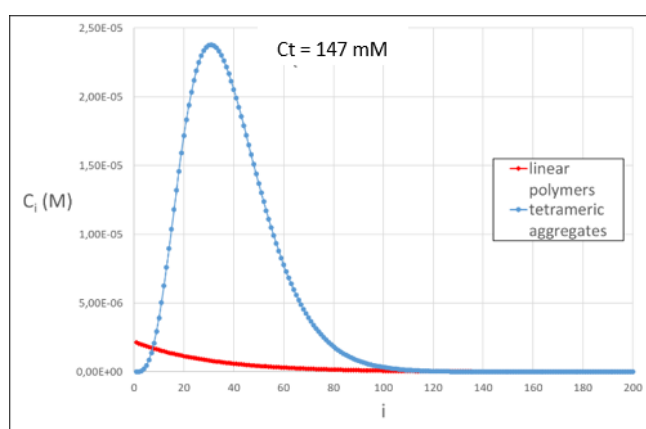


Figure 8. Distribution of linear polymeric chains (red circles) and four chains bundle aggregates (blue circles) obtained using the SEK-TAi<sup>4</sup> model, with  $K_{SEK}$  ( $4.55 \times 10^5 \text{ M}^{-1}$ ) and  $K_{TA4}$  ( $6.13 \times 10^{13} \text{ M}^{-3}$ ) values optimized to fit the experimental PGSE measurements for a monomer concentration of 147 mM.

In particular, the SEK-TAi<sup>4</sup> model, having the best fit of PGSE data (Figure 7), shows a maximum value of the average degree of polymerization of 146 for a total monomer concentration of 147 mM. The corresponding value for the SEK-TAi model is 121 and 103 for the pure SEK model (Figure 9).

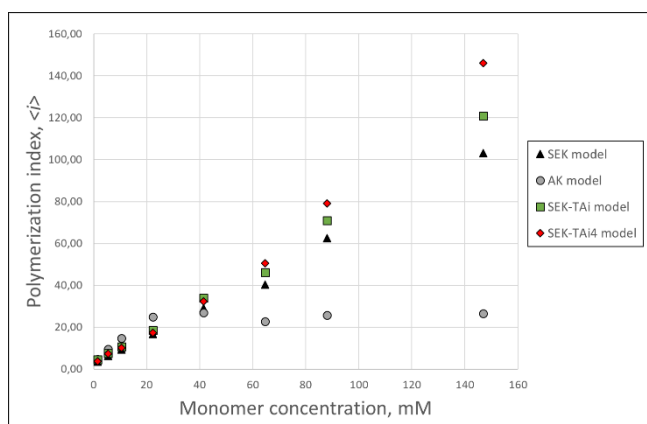


Figure 9. Comparison between the calculated average degree of polymerization obtained from distributions of polymeric species in four different models, i.e. SEK (black triangles), AK (grey circles), SEK-TAi (green squares) and SEK-TAi<sup>4</sup> (red diamonds).

## Electrochemical properties

The electrochemical properties of the systems **1**<sup>+</sup>, **3**<sup>+</sup>, **4•3**<sup>+</sup> and **4•5**<sup>+</sup> were explored by means of cyclic voltammetry (CV), differential pulse voltammetry (DPV) and spectroelectrochemical measurements.

The aim of this study is to understand the electrochemical behaviour of the homopolymer **1** on the basis of the results obtained from the investigation of the system **4•5** which constitutes a good model for the host-guest association that leads to supramolecular polymerization.<sup>23</sup> In fact, the results obtained in that case were promising about the possibility of controlling electrochemically the self-assembly of the supramolecular polymer.

The electroactive unit of the monomer **1** is the MePy<sup>+</sup> moiety, whose electrochemical behaviour is known both when it is free and complexed by the P=O groups of the tetraphosphonate cavitand (see system **4•5**). In order to obtain an even better model for the system **1**, we performed electrochemical experiments on the thio-systems **3CF<sub>3</sub>SO<sub>3</sub>** and dimeric **4•3CF<sub>3</sub>SO<sub>3</sub>**.

## Model systems

Cavitand **3** constitutes a good model for the study of the electrochemical properties of the MePy<sup>+</sup> unit of the monomer **1** when it is not complexed by the P=O groups in the polymeric structure.

This species exhibits a reversible reduction process at  $-0.69 \text{ V vs SCE}$  (Figure S13), clearly assigned to the first reduction of its MePy<sup>+</sup> unit by comparison with compound **5**. At potentials more negative than  $-1.2 \text{ V}$  there are overlapping irreversible waves, most likely due to reduction of the P=S groups, which prevent the observation of the second reduction process of the methylpyridinium unit, expected at around  $-1.6 \text{ V}$ . The DPV measurements confirm these observations.

The electrochemical behaviour of the complex **4•3** (Figure S14), which should reflect the properties of the MePy<sup>+</sup> unit of the monomer **1** when it is complexed by the P=O groups in the supramolecular polymer, is qualitatively similar to that of system **3**. The reversible wave at  $-0.75 \text{ V vs SCE}$  is assigned to the first monoelectronic reduction of the MePy<sup>+</sup> unit of **3**, which occurs at  $-0.69 \text{ V}$  in the absence of the P=O cavitand. Such a negative shift can be interpreted in terms of the stabilization offered by the cavity of the P=O cavitand to the MePy<sup>+</sup> unit of **3**, in agreement with the results obtained for the **4•5** model system (Table 3).<sup>23</sup>

As observed for **3** alone, the second reduction process of the MePy<sup>+</sup> unit is hidden by intense irreversible waves at potentials more negative than  $-1.2 \text{ V}$ , assigned to the reduction of the P=S cavitand moiety. Therefore, the voltammetry data yield no indication on the fate of the complex after monoelectronic reduction of **3**. On the basis of the strict similarity of this system with **4•5**, it is reasonable to expect that one-electron reduction of the MePy<sup>+</sup> unit leads to substantial disassembly of the complex.<sup>23</sup> The apparent reversibility of the CV wave shown in Figure 11 indicates that the chemical rearrangements possibly associated with the electrochemical processes are fast on the cyclic voltammetry time scale.

Table 3. Electrochemical data for the two reduction processes of the MePy<sup>+</sup> unit in the investigated compounds (CH<sub>2</sub>Cl<sub>2</sub>/TBAPF<sub>6</sub>, room temperature, glassy carbon electrode; ferrocene was used as an internal reference, E(Fc<sup>+</sup>/Fc) = +0.46 V vs SCE).

System	E <sup>1</sup> /V vs SCE	E <sup>2</sup> /V vs SCE
3	-0.69[a]	[b]
4•3	-0.75[a]	[b]
5	-0.70[a]	-1.57[c]
4•5	-0.80[c]	-1.57[c]
1	-0.75[c], -1.19[c]	-1.50[c,d]

[a] Half wave potential values of reversible process. [b] The voltammetry signal for the MePy<sup>+</sup> second reduction is covered by overlapping irreversible peaks ascribed to reduction of the P=S moieties of the cavitand. [c] Chemically irreversible process; potential value estimated from the DPV peak at a scan rate of 20 mV/s. [d] Strongly affected by electrode adsorption.

### Supramolecular polymer **11**

In the examined potential window, the self-assembling system **11** undergoes three chemically irreversible reduction processes (Figure 10). All of them have to be attributed to the MePy<sup>+</sup> unit, which is the sole electroactive unit of **1**. The reduction potentials obtained from the DPV peaks are -0.75 V, -1.19 V, and -1.50 V vs SCE, respectively (Table 3).

In the CV, because of the chemical irreversibility of the processes, we consider the potential values of the cathodic peaks. The CV of the solution with [**1**] = 0.64 mM shows three cathodic peaks at -0.78 V, -1.22 V and -1.53 V vs SCE, respectively. The waves at -0.78 V and -1.53 V can be unambiguously attributed to the first and second reduction processes of the MePy<sup>+</sup> unit, respectively, by comparison with model systems. The first reduction wave occurs at a potential consistent with a MePy<sup>+</sup> unit encircled by the cavitand,<sup>23</sup> in agreement with the fact that under the conditions employed the vast majority of **1** species are self-assembled into polymeric aggregates **11**.<sup>19</sup>

The reduction process responsible for the cathodic wave at -1.22 V cannot be straightforwardly assigned. To understand the origin of this process we performed further CV studies upon changing the monomer concentration (Figure 10) and the potential scan rate (Figure 11).

Upon increasing the concentration of **1** it can be noticed that the peak at -1.22 V grows in intensity at the expense of the peak at -0.78 V (Figure 10) which, at the same time, improves its chemical reversibility (see the anodic wave at ca. -0.70 V). The same qualitative changes in the CV pattern – i.e., the relative increase of the peak at -1.22 V compared with that at -0.78 V and the enhancement of the chemical reversibility of the first reduction process – are observed on increasing the potential scan rate (Figure 11). This picture can be interpreted considering that the polymer chains **11** can associate together side-by-side to generate bundles stabilized by a combination of multipole interactions and Van der Waals forces. In solution such bundle-like structures are in equilibrium with the non-aggregated polymer chains.

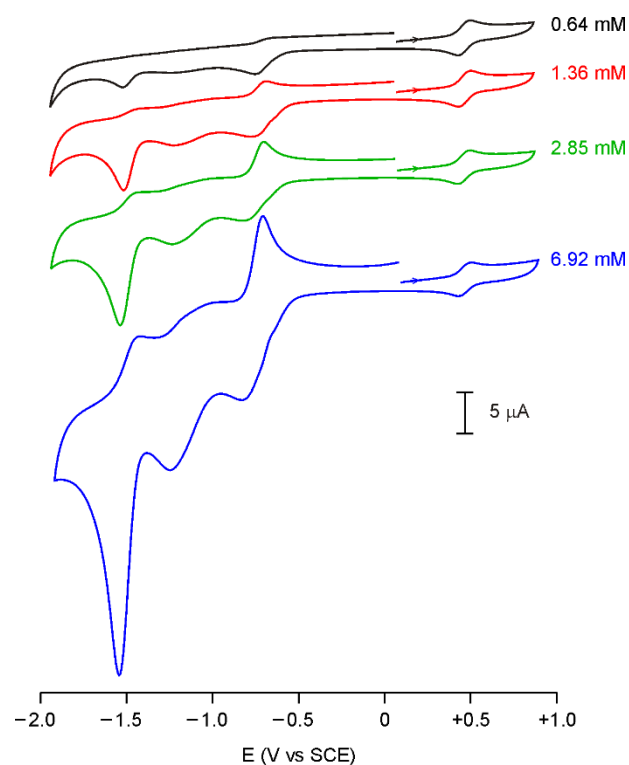


Figure 10. Cyclic voltammograms for the reduction of the homopolymer **11** at various monomer **1** concentrations (CH<sub>2</sub>Cl<sub>2</sub> with 0.68 M TBAPF<sub>6</sub>, glassy carbon electrode, scan rate 200 mV/s). The reversible wave at +0.46 V vs SCE is that of ferrocene used as an internal standard.

Because the cationic pyridinium units along the chains are strongly involved in the multipole interactions responsible for the formation of the bundles, it can be expected that the MePy<sup>+</sup> moieties belonging to polymer chains associated in a bundle are stabilized, and hence become more difficult to reduce, compared to units belonging to non-aggregated polymer chains.

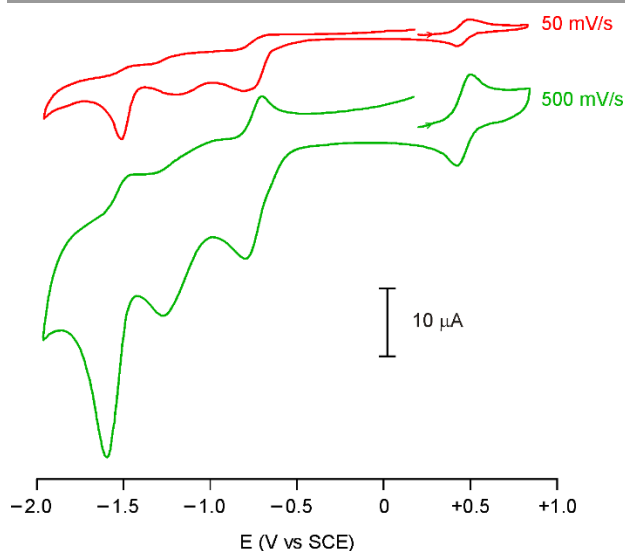


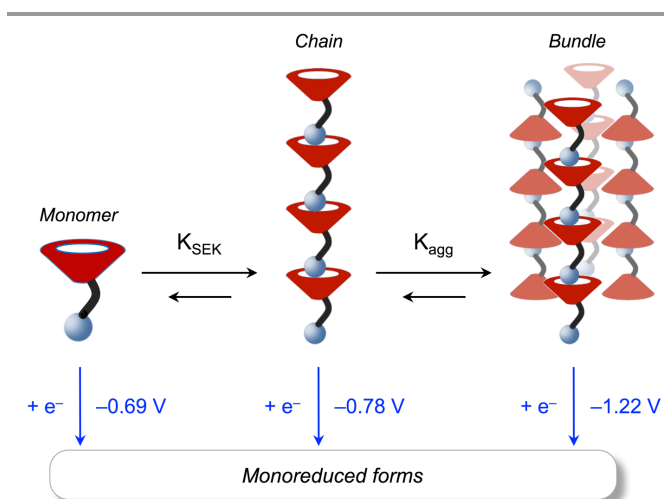
Figure 11. Cyclic voltammograms for the reduction of homopolymer **11** at different scan rates (monomer concentration 5.04 mM, CH<sub>2</sub>Cl<sub>2</sub> with 0.51 M TBAPF<sub>6</sub>, glassy carbon electrode). The reversible wave at +0.46 V vs SCE is that of ferrocene used as an internal standard.

Therefore, while the process at  $-0.78$  V is assigned to cavitand-complexed MePy<sup>+</sup> units in non-aggregated chains, the one at  $-1.22$  V is attributed to cavitand-complexed MePy<sup>+</sup> units in bundled chains (Scheme 2).

Such an interpretation is fully consistent with the observed CV behaviour. The intensity ratio of the peaks assigned to reduction of bundles and single chains is expected to increase at higher monomer concentrations, when the equilibrium is more displaced towards the formation of the bundles. This is exactly what is observed in the experiments (Figure 10). Because there is a chemical equilibrium between bundled and unbundled polymer chains, the reduction of the MePy<sup>+</sup> units in the non-associated chains at  $-0.78$  V is expected to shift the equilibrium away from the bundled structure towards the unbundled one. In fact, upon increasing the potential scan rate, the cathodic peak at  $-1.22$  V is enhanced (Figure 11) because the disruption of the bundles in consequence of the first reduction ( $-0.78$  V) becomes slow in the time scale of the electrochemical experiment. Conversely, the equilibrium shift leading to a decrease of the concentration of the bundles (and hence of the corresponding current intensity at  $-1.22$  V) can be observed at slower scan rates (Figure 11).

At this point, it should be assessed whether the first reduction of the MePy<sup>+</sup> unit of **1** leads to the disassembly of the polymer, as it happens for the **4•5** model system. In the case of **11**, however, the potential for the second reduction process of the MePy<sup>+</sup> unit does not give a clear indication about the fate of the aggregate after the first reduction. To this aim we performed spectroelectrochemical measurements on cavitand **3** and polymer **11**.

The absorption spectrum of the monoreduced **3** species, obtained upon electrolysis of **3** at  $-1.0$  V vs an Ag pseudo-reference electrode, shows two intense bands with  $\lambda_{\text{max}} = 304$  and  $395$  nm (Figure 12a) that are characteristic of the monoreduced MePy unit. The absorption spectrum obtained upon electrolysis of a solution of polymer **11** at  $-1.33$  V vs an Ag pseudo-reference electrode (Figure 12b) shows the same bands



Scheme 2. Representation of the self-assembly processes of polymer chains **11** and bundle aggregates (**11**)<sub>n</sub> from monomer **1**, and associated electrochemical one-electron reduction of their MePy<sup>+</sup> units. The potential value for the reduction of the MePy<sup>+</sup> unit in model compound **3** is taken as the reduction potential of monomeric **1**.

observed for the monoreduced **3** species. If the monoreduced MePy moiety remained included in the cavitand, it is reasonable to assume that the absorption spectrum of the former would be affected in some way. Hence, the spectroelectrochemical results suggest that the polymer is disassembled upon one-electron reduction of the MePy<sup>+</sup> moiety.

The CV cathodic wave at  $-1.53$  V, assigned to the second reduction of the MePy<sup>+</sup> units, is strongly affected by electrode adsorption phenomena for scan rates higher than  $50$  mV/s. Such a behaviour suggests that under these conditions the monoreduced species precipitate onto the electrode surface. The potential for this process, however, can be reasonably estimated at a slow scan rate ( $20$  mV/s) by DPV measurements (Table 3). It is interesting to note that the process takes place at a less negative potential ( $-1.50$  V) compared to the same process in a free MePy<sup>+</sup> ( $-1.57$  V). This observation might indicate that the **1** species, which become non-associated in their neutral form (i.e. after one-electron reduction of their MePy<sup>+</sup> units, vide supra), self-assemble again in their negatively charged form (i.e. upon two-electron reduction). The stability of the resulting aggregate would account for the fact that the second reduction of **1** is easier than that of model compound **5**, leading to a positive shift in the corresponding redox potential.

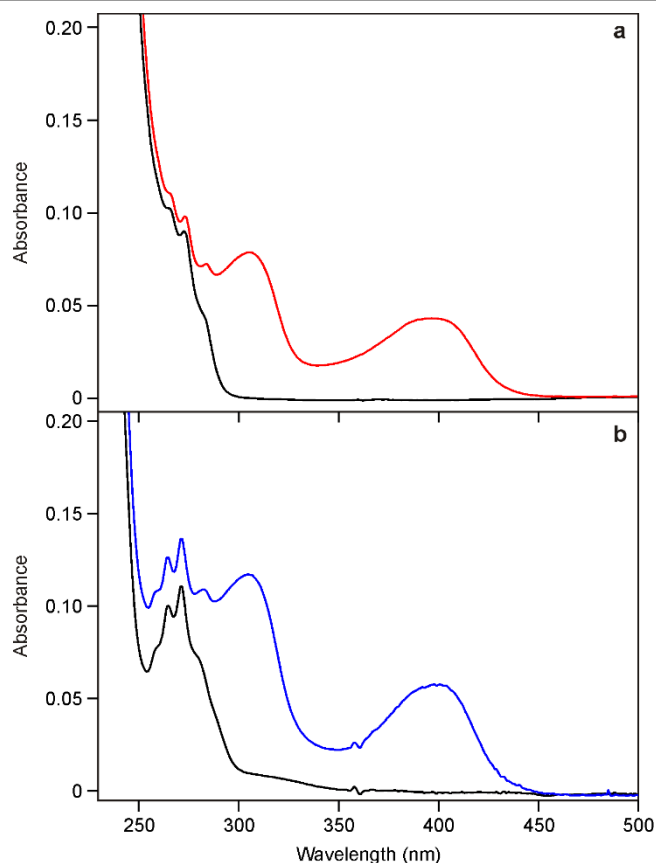


Figure 12. (a) Absorption spectrum of **3** before (black line) and after (red line) exhaustive electrolysis at  $-1.0$  V. Conditions:  $0.839$  mM,  $\text{CH}_2\text{Cl}_2/86.0$  mM TBAPF<sub>6</sub>. (b) Absorption spectrum of the supramolecular polymer **11** before (black line) and after (blue line) exhaustive electrolysis at  $-1.33$  V. Conditions: monomer concentration  $0.706$  mM,  $\text{CH}_2\text{Cl}_2/73.4$  mM TBAPF<sub>6</sub>. Platinum grid working electrode, Ag pseudo-reference electrode, optical path length  $180$   $\mu\text{m}$ .

Our data are insufficient to allow speculations about the nature of these aggregates, but their formation cannot be simply explained in terms of host-guest interactions between a doubly reduced MePy moiety and a P=O cavitand, because the **4•5** model system shows a different behaviour.

In summary, the self-assembly equilibrium leading to the formation of the supramolecular polymer **11** can be controlled electrochemically (Scheme 2); specifically, one-electron reduction of the MePy<sup>+</sup> unit of **1** causes the disassembly of the polymer. The reversibility of the switching process, however, is limited by the poor chemical reversibility of the MePy<sup>+</sup> reduction. In addition, voltammetry measurements suggest that the polymer chains **11** undergo aggregation, in line with the NMR results.

## Conclusions

The overall picture emerging from the NMR and voltammetry experiments supported by theoretical models, shows that: i) below 20 mM monomer concentration, the main aggregation process is the isodesmic linear polymerization of cavitand **1**; ii) above 20 mM, dipolar and quadrupolar interactions involving longer linear chains become energetically relevant. At high monomer concentration (147 mM) tetrameric bundles, formed by the antiparallel aggregation of four linear chains, prevails, as inferred by the non-linear fitting of the PGSE data obtained using the SEK-TAi<sup>4</sup> model (Fig S13). Interestingly, the bundles assembly results in a ten-fold increase of the K<sub>SEK</sub>, showing a synergistic effect on aggregation process between linear polymerization and bundle assembly. Furthermore, the bundle formation increases the stability of the linear chains toward electrochemical reduction. The different nature of the weak interactions of the two assembly modes allowed to devise two orthogonal disassembly procedures. The dipolar and quadrupolar interactions leading to bundle aggregation are more sensitive to solvent polarity than the host-guest interactions. On the other hand, bundles are more stable than linear chains toward electrochemical reduction. Tuning either one of the two stimuli allows to control the equilibrium toward the desired species.

## Conflicts of interest

There are no conflicts to declare.

## Acknowledgements

Financial support from the Italian Ministry of University and Research (PRIN 2017 projects 20179BJNA2 and 20173L7W8K), and the European Union (H2020 FET-OPEN “Magnify” no. 801378) is gratefully acknowledged.

This work has benefited from the equipment and framework of the COMP-HUB Initiative of the University of Parma and AMIS from University of Udine, funded by the ‘Departments of Excellence’ program of the Italian Ministry for Education, University and Research (MIUR, 2018-2022).

## Notes and references

- 1 Roy, N.; Bruchmann, B.; Lehn, J.-M., DYNAMERS: dynamic polymers as self-healing materials. *Chem. Soc. Rev.* 2015, 44, 3786-3807.
- 2 Zhang, Y.; Barboiu, M., Constitutional Dynamic Materials—Toward Natural Selection of Function. *Chem. Rev.* 2016, 116, 809-834.
- 3 Aida, T.; Meijer, E. W.; Stupp, S. I., Functional supramolecular polymers. *Science* 2012, 335, 813-817.
- 4 Goor, O. J. G. M.; Hendrikse, S. I. S.; Dankers, P. Y. W.; Meijer, E. W., From supramolecular polymers to multi-component biomaterials. *Chem. Soc. Rev.* 2017, 46, 6621-6637.
- 5 Webber, M. J.; Appel, E. A.; Meijer, E. W.; Langer, R., Supramolecular biomaterials. *Nat. Mater.* 2015, 15, 13-26.
- 6 Lu, Y.; Aimetti, A. A.; Langer, R.; Gu, Z., Bioresponsive materials. *Nat. Rev. Mater.* 2016, 2, 16075.
- 7 Ouchi, H.; Kizaki, T.; Yamato, M.; Lin, X.; Hoshi, N.; Silly, F.; Kajitani, T.; Fukushima, T.; Nakayama, K.-I.; Yagai, S., Impact of helical organization on the photovoltaic properties of oligothiophene supramolecular polymers. *Chem. Sci.* 2018, 9, 3638-3643.
- 8 Fouquey, C.; Lehn, J.-M.; Levelut, A.-M., Molecular recognition directed self-assembly of supramolecular liquid crystalline polymers from complementary chiral components. *Adv. Mater.* 1990, 2, 254-257.
- 9 Balzani, V.; Campagna, S.; Denti, G.; Juris, A.; Serroni, S.; Venturi, M., Designing Dendrimers Based on Transition-Metal Complexes. Light-Harvesting Properties and Predetermined Redox Patterns. *Acc. Chem. Res.* 1998, 31, 26-34.
- 10 Li, S.-L.; Xiao, T.; Lin, C.; Wang, L., Advanced supramolecular polymers constructed by orthogonal self-assembly. *Chem. Soc. Rev.* 2012, 41, 5950-5968.
- 11 Harada, A.; Takashima, Y.; Nakahata, M., Supramolecular Polymeric Materials via Cyclodextrin-Guest Interactions. *Acc. Chem. Res.* 2014, 47, 2128-2140.
- 12 Liu, J.; Tan, C. S. Y.; Lan, Y.; Scurman, O. A., Aqueous Polymer Self-Assembly Based on Cucurbit[n]uril-Mediated Host-Guest Interactions. *Macromol. Chem. Phys.* 2016, 217, 319-332.
- 13 Li, H.; Yang, Y.; Xu, F.; Liang, T.; Wen, H.; Tian, W., Pillararene-based supramolecular polymers, *Chem. Commun.* 2019, 55, 271-285.
- 14 a) Haino, T.; Matsumoto, Y.; Fukazawa, Y., Supramolecular Nano Networks Formed by Molecular-Recognition-Directed Self-Assembly of Ditopic Calix[5]arene and Dumbbell [60]Fullerene. *J. Am. Chem. Soc.* 2005, 127, 8936-8937; b) Capici, C.; Cohen, Y.; D’Urso, A.; Gattuso, G.; Notti, A.; Pappalardo, A.; Pappalardo, S.; Parisi, M. F.; Purrello, R.; Slovak, S.; Villari, V. Anion-assisted Supramolecular Polymerization: from Achiral AB-type Monomers to Chiral Assemblies. *Angew. Chem. Int. Ed.* 2011, 50, 11956-11961.
- 15 Guo, D.-S.; Liu, Y., Calixarene-based supramolecular polymerization in solution, *Chem. Soc. Rev.* 2012, 41, 5907-5921.
- 16 Tancini, F.; Dalcanale, E. Polymerization with Ditopic Cavitand Monomers. *Supramolecular Polymer Chemistry* (Ed. A. Harada), Wiley-VCH Verlag GmbH & Co. KGaA, Weinheim, Germany, 2012, 71-93.
- 17 Pironcini, L.; Stendardo, A. G.; Geremia, S.; Campagnolo, M.; Samori, P.; Rabe, J. P.; Fokkens, R.; Dalcanale, E., Dynamic materials through metal-directed and solvent-driven self-assembly of cavitands. *Angew. Chem. Int. Ed.* 2003, 42, 1384-1387.
- 18 Nitta, N.; Takatsuka, M.; Kihara, S.; Hirao, T.; Haino, T., Self-Healing Supramolecular Materials Constructed by Copolymerization via Molecular Recognition of Cavitand-based Coordination Capsules. *Angew. Chem. Int. Ed.* 2020, 10.1002/anie.202006604.

- 19 Yebeutchou, R. M.; Tancini, F.; Demitri, N.; Geremia, S.; Mendichi, R.; Dalcanale, E., Host-guest driven self-assembly of linear and star supramolecular polymers. *Angew. Chem. Int. Ed.* 2008, 47, 4504-4508.
- 20 Tancini, F.; Yebeutchou, R. M.; Pirondini, L.; Dezorzi, R.; Geremia, S.; Scherman, O. A.; Dalcanale, E., Host-guest-driven copolymerization of tetrakisphosphonate cavitands. *Chem. Eur. J.* 2010, 16, 14313-14321.
- 21 Dionisio, M.; Ricci, L.; Pecchini, G.; Masseroni, D.; Ruggeri, G.; Cristofolini, L.; Rampazzo, E.; Dalcanale, E., Polymer Blending through Host-Guest Interactions. *Macromolecules* 2014, 47, 632-638.
- 22 Masseroni, D.; Rampazzo, E.; Rastrelli, F.; Orsi, D.; Ricci, L.; Ruggeri, G.; Dalcanale, E. pH-responsive host-guest polymerization and blending. *RSC Adv.* 2015, 5, 11334-11342.
- 23 Gadenne, B.; Semeraro, M.; Yebeutchou, R. M.; Tancini, F.; Pirondini, L.; Dalcanale, E.; Credi, A., Electrochemically Controlled Formation/Dissociation of Phosphonate-Cavitand/Methylpyridinium Complexes. *Chem. Eur. J.* 2008, 14, 8964-8971.
- 24 Jeener, J.; Meier, B. H.; Bachmann, P.; Ernst, R. R., Investigation of exchange processes by two-dimensional NMR spectroscopy. *J. Chem. Phys.* 1979, 71, 4546-4553.
- 25 Wagner, R.; Berger, S., Gradient-Selected NOESY—A Fourfold Reduction of the Measurement Time for the NOESY Experiment. *J. Magnet. Res., Series A* 1996, 123, 119-121.
- 26 a) Lix, B.; Sönnichsen, F. D.; Sykes, B. D., The Role of Transient Changes in Sample Susceptibility in Causing Apparent Multiple-Quantum Peaks in HOESY Spectra. *J. Magnet. Res., Series A* 1996, 121, 83-87; b) Menozzi, E.; Busi, M.; Messera, C.; Ugozzoli, F.; Zuccaccia, D.; Macchioni, A.; Dalcanale, E. "Metal-Directed Self-Assembly of Cavitand Frameworks" *J. Org. Chem.* 2006, 71, 2617-2624.
- 27 a) Perrin, C. L.; Dwyer, T. J., Application of two-dimensional NMR to kinetics of chemical exchange. *Chem. Rev.* 1990, 90, 935-967; b) Zuccaccia, D.; Pirondini, L.; Pinalli R.; Dalcanale, E.; Macchioni, A. "Dynamic and Structural NMR Studies of Cavitand-Based Coordination Cages", *J. Am Chem. Soc.* 2005, 127, 7025-7032.
- 28 Zuccaccia, D.; Macchioni, A., An Accurate Methodology to Identify the Level of Aggregation in Solution by PGSE NMR Measurements: The Case of Half-Sandwich Diamino Ruthenium(II) Salts. *Organometallics* 2005, 24, 3476-3486; b) Macchioni, A.; Ciancaleoni, G.; Zuccaccia, C.; Zuccaccia, D., Determining accurate molecular sizes in solution through NMR diffusion spectroscopy. *Chem. Soc. Rev.* 2008, 37, 479-489; c) Pregosin, P. S.; Kumar, P. G. A.; Fernández, I. Pulsed Gradient Spin-Echo (PGSE) Diffusion and  $^1\text{H}$ ,  $^{19}\text{F}$  Heteronuclear Overhauser Spectroscopy (HOESY) NMR Methods in Inorganic and Organometallic Chemistry: Something Old and Something New. *Chem. Rev.* 2005, 105, 2977-2998.
- 29 Schlögl, R., H. J. Tyrell, K. R. Harris: Diffusion in Liquids, A Theoretical and Experimental Study. *Berichte der Bunsengesellschaft für physikalische Chemie* 1985, 89, 209-210.
- 30 Mills, R., Self-diffusion in normal and heavy water in the range 1-45 deg. *J. Phys. Chem.* 1973, 77, 685-688.
- 31 Eaton, J. W., GNU Octave and reproducible research. *J. Process Control* 2012, 22, 1433-1438.
- 32 a) Cohen, Y.; Slovak, S. Diffusion NMR for the characterization, in solution, of supramolecular systems based on calixarenes, resorcinarenes, and other macrocyclic arenes *Org. Chem. Front.*, 2019, 6, 1705-1718; b) Zaccaria, F.; Zuccaccia, C.; Cipullo, R.; Macchioni, A. Extraction of Reliable Molecular Information from Diffusion NMR Spectroscopy: Hydrodynamic Volume or Molecular Mass? *Chem Eur. J.* 2019, 25, 9930-9937; c) Cohen, Y.; Avram, L.; Evan-Salem, T.; Slovak, S.; Shemesh N.; Frish, L. Analytical Methods in Supramolecular Chemistry, ed. C. A. Schalley, Wiley-VCH, Berlin, 2nd edn, 2012, vol. 1, ch. 7, pp. 197-286; d) P. Stilbs, *Prog. Nucl. Magn. Reson. Spectrosc.*, 1987, 17, 1-45; e) Y. Cohen, L. Avram and L. Frish, *Angew. Chem., Int. Ed.* 2005, 44, 520-554.
- 33 a) Macchioni, A., Elucidation of the Solution Structures of Transition Metal Complex Ion Pairs by NOE NMR Experiments. *Eur. J. Inorg. Chem.* 2003, 195-205; b) Macchioni, A.; Magistrato, A.; Orabona, I.; Ruffo, F.; Rothlisberger, U.; Zuccaccia, C. Direct observation of an equilibrium between two anion-cation orientations in olefin Pt(II) complex ion pairs by HOESY NMR spectroscopy. *New J. Chem* 2003, 27, 455-458; c) Biasiolo L.; Ciancaleoni G.; Belpassi L.; Bistoni G.; Macchioni A.; Tarantelli F.; Zuccaccia D. 'Relationship between the anion/cation relative orientation and the catalytic activity of nitrogen acyclic carbene-gold catalysts' *Catal. Sci. Technol.*, 2015, 5, 1558-1567.
- 34 Bellachioma, G.; Ciancaleoni, G.; Macchioni, A.; Zuccaccia, C.; Zuccaccia, D. "NMR investigation of non-covalent aggregation of coordination compounds ranging from dimers and ion pairs up to nano-aggregates" *Coord. Chem. Rev.* 2008, 252, 2224-2248.
- 35 a) Garland, F.; Christian, S. D., Thermodynamic and kinetic model of sequential nucleoside base aggregation in aqueous solution. *J. Phys. Chem.* 1975, 79, 1247-1252; b) Martin, R. B. Comparisons of Indefinite Self-Association Models *Chem. Rev.* 1996, 96, 3043-3064; c) Rocchigiani, L.; Bellachioma, G.; Ciancaleoni, G.; Crocchianti, S.; Lagana, A.; Zuccaccia, C.; Zuccaccia, D.; Macchioni, A. Anion-Dependent Tendency of Di-Long-Chain Quaternary Ammonium Salts to Form Ion Quadruples and Higher Aggregates in Benzene *ChemPhysChem* 2010, 11, 3243-3254.
- 36 (36) Garcia de la Torre, J.; Navarro, S.; Lopez Martinez, M. C.; Diaz, F. G.; Lopez Cascales, J. J., HYDRO: a computer program for the prediction of hydrodynamic properties of macromolecules. *Biophys. J.* 1994, 67, 530-531.
- 37 Perrin, F., Mouvement brownien d'un ellipsoïde - I. Dispersion diélectrique pour des molécules ellipsoïdales. *J. Phys. Radium* 1934, 5, 497-511.
- 38 Menozzi, D.; Biavardi, E.; Massera, C.; Schmidtchen, F.-P.; Cornia, A.; Dalcanale, E., Thermodynamics of Host-Guest Interactions Between Methylpyridinium Salts and Phosphonate Cavitands. *Supramol. Chem.* 2010, 22, 768-775.